Climate Dynamics (2024) 62:3763–3781
https://doi.org/10.1007/s00382-023-07097-8

ORIGINAL ARTICLE

SPEEDY-NEMO: performance and applications of a fully-coupled intermediate-complexity climate model

Paolo Ruggieri[1] · Muhammad Adnan Abid[2,4] · Javier García-Serrano[3] · Carlo Grancini[1] · Fred Kucharski[2] · Salvatore Pascale[1] · Danila Volpi[3]

Received: 1 August 2023 / Accepted: 26 December 2023 / Published online: 7 February 2024

Abstract
A fully-coupled general circulation model of intermediate complexity is documented. The study presents an overview of the model climatology and variability, with particular attention to the phenomenology of processes that are relevant for the predictability of the climate system on seasonal-to-decadal time-scales. It is shown that the model can realistically simulate the general circulation of the atmosphere and the ocean, as well as the major modes of climate variability on the examined time-scales: e.g. El Niño-Southern Oscillation, North Atlantic Oscillation, Tropical Atlantic Variability, Pacific Decadal Variability, Atlantic Multi-decadal Variability. Potential applications of the model are discussed, with emphasis on the possibility of generating sets of low-cost large-ensemble retrospective forecasts. We argue that the presented model is suitable to be employed in traditional and innovative model experiments that can play a significant role in future developments of seasonal-to-decadal climate prediction.

Keywords Intermediate-complexity climate model · Seasonal-to-decadal variability · Climate predictions

1 Introduction

General circulation models (GCMs) of intermediate complexity (IC) have been developed for decades with the overarching goal of understanding the processes that govern Earth's climate and its variability. Models of this kind have been used extensively in the scientific literature (e.g., Hoskins 1993; Fraedrich et al. 2005; Smith et al. 2008; Schmittner et al. 2011; Williams et al. 2014; Joshi et al. 2015; Holden et al. 2016; Platov et al. 2017; Maher et al. 2019) and their value has been highlighted by a number of reviews and perspectives (see for instance Held 2005; Nof 2008; Weber 2010; Kucharski et al. 2013, and references therein). Recent studies further documented the development of IC climate models for a range of applications. For instance, Blaker et al. (2021) presented a novel version of an IC model aimed at studying physical processes and climate variability at decadal-to-centennial time-scales, while Horak et al. (2021) described an IC mesoscale atmospheric model and Molteni et al. (2023) presented an IC climate model with a thermodynamic ocean. A renewed interest for model hierarchies of different complexity is documented in the recent works of Jeevanjee et al. (2017), Maher et al. (2019), Balaji (2021), and Marques et al. (2022).

These studies testify a long-lived and ongoing effort of the community to build modelling tools for specific applications that lie between simplified conceptual models and high-complexity models.

Specific questions related to anthropogenic climate change on the scale of many decades and centuries (e.g., Forest et al. 2002, and references therein] have been explored thoroughly with the help of IC climate models. More recently, the phenomenology and processes of climate variability on seasonal-to-decadal (S2D) time-scales have gained growing attention to support the development of operational predictions. The representation of physical processes that are fundamental for skilful S2D predictions

✉ Paolo Ruggieri
paolo.ruggieri2@unibo.it

[1] Department of Physics and Astronomy, University of Bologna, Via Irnerio 46, Bologna, Italy

[2] The Abdus Salam International Centre for Theoretical Physics (ICTP), Trieste, Italy

[3] Group of Meteorology, Universitat de Barcelona, Barcelona, Spain

[4] Atmosphere, Oceanic and Planetary Physics (AOPP), Department of Physics, University of Oxford, Oxford, UK

is thought to require relatively complex models. For instance, seasonal prediction skill in operational forecasts, particularly over land in the extra-tropics, is deemed to be the result of a combination of predictable processes involving variability in tropical sea surface temperature (Domeisen et al. 2015), sea-ice (Seidenglanz et al. 2021), land-cover (Ruggieri et al. 2022) and the stratosphere (Nie et al. 2019). Similarly, on a multi-year range, prediction skill arises from oceanic and non-oceanic sources of predictability (Bellucci et al. 2015). In many cases, predictable components of the climate system lead to forecast skill over land via atmospheric teleconnections that originate in oceanic regions and affect remotely the state of meteorological variables through a chain of processes that invoke the need for high-end numerical models. Indeed, S2D forecasts represent a coordinated effort with an ongoing tendency to combine high spatial resolution and large ensembles in multi-model coupled simulations with GCMs. Arguably this effort has been instrumental to the development of operational S2D forecasts that nowadays reveal skilful predictions (Smith et al. 2019, 2020, e.g.,) relevant for sectoral applications (Dunstone et al. 2022). The effect on the prediction skill coming from enhanced horizontal resolution has been assessed but its added value is not conclusive (e.g., Scaife et al. 2019; Haarsma et al. 2020). Indeed, Merryfield et al. (2020) recently outlined a roadmap for the development of S2D predictions that involves further research in initialisation methods, ensemble generation techniques and reduction of model bias. They note that, even though increasing model resolution might be a rewarding exercise, the development of S2D prediction requires research strategies to understand how models behave in representing the predictable processes that lead to forecast skill. In this context, IC models can be useful to tackle research questions that are currently investigated by the community dealing with the advancement of S2D prediction, particularly when large-scale dynamics and low-frequency variability are involved.

In this study, we document the formulation, climatology and variability of a fully-coupled intermediate-complexity GCM. The model, named SPEEDY-NEMO, is based on the coupling of an intermediate-complexity atmospheric GCM and a low-resolution ocean/sea-ice model, which is designed to achieve a compromise between resolution, complexity and computational cost while maintaining a realistic representation of the climate system. Early versions of the model have already been reported sporadically in the scientific literature (Kucharski et al. 2016; Sluka et al. 2016; Justino et al. 2019; Kalnay et al. 2023), but a comprehensive review of the coupled model climatology and variability is missing. We show that the model yields a realistic simulation of ocean–atmosphere modes of S2D variability. It is argued that the presented model can be applied to investigate a range of scientific questions that are relevant to the understanding of S2D predictability and the development of S2D predictions.

After this introduction, in Sect. 2 we describe the model formulation with reference to previous studies, the setup of the simulations performed in this study and data used for the model validation. Section 3 presents the analysis of a model run with stationary forcing, with emphasis on the main aspects of the atmospheric-oceanic general circulation, surface climate and variability on S2D time-scales. Section 4 discusses potential applications of the model. Finally in Sect. 5 we summarise the main findings of the study.

2 Data and methods

2.1 The model

This study documents an intermediate complexity coupled GCM, hereafter called SPEEDY-NEMO. The atmosphere component is SPEEDY (Simplified Parameterizations, privitivE-Equation Dynamics, Molteni 2003; Kucharski et al. 2006, 2013) that is based on the hydrostatic spectral dynamical core originally developed by Held and Suarez (1994). The time stepping is based on a leapfrog scheme with a Robert-Asselin filter (Robert 1966; Asselin 1972) to damp the computational mode and the RAW filter (Amezcua et al. 2011) to increase the accuracy. The model is run with a triangular spectral truncation at wavenumber 30 (T30, but note that a version at T47 is already developed and available) on a gaussian grid of 96×48 points (longitude×latitude). The prognostic variables of the model are temperature, specific humidity, vorticity, divergence and logarithm of surface pressure. The 3-dimensional prognostic variables are evaluated on 8 σ-coordinate layers with $\sigma = 0.025, 0.095, 0.20, 0.34, 0.51, 0.685, 0.835$ and 0.95. Here $\sigma = p/p_s$ where p is pressure and p_s is surface pressure. The model output used in this manuscript is interpolated on pressure levels at 30, 100, 200, 300, 500, 700, 850 and 925 hPa. The model includes parameterisations of radiation, convection, vertical diffusion, surface heat and momentum fluxes, clouds and large-scale condensation. A detailed description of the model formulation is provided in a technical report (http://users.ictp.it/~kucharsk/speedy_description/km_ver41_appendixA.pdf).

The ocean component is the Nucleus for European Modelling of the Ocean (NEMO) v.3.0 (Madec 2008). The model solves the primitive equations with the hydrostatic and Boussinesq approximations. The equations are solved on a tripolar ORCA2 grid with horizontal resolution of about 2° and a tropical refinement up to 0.5°. The model has 31 vertical levels (z coordinate) with a thickness ranging from 10 m at the surface to 500 m at the ocean bottom. SPEEDY-NEMO includes the Louvain-la-Neuve sea ice model (LIM)

which is a dynamic-thermodynamic model with a snow layer and two ice layers for sensible heat storage and vertical heat conduction within snow and ice. Energy budgets at the upper and lower surfaces and lead surfaces drive vertical and lateral sea ice change rates. The subgrid snow and ice thickness distributions are parametrized by means of an effective thermal conductivity. Storage of latent heat inside the ice resulting from the trapping of shortwave radiation is modelled and a surface albedo is parameterized. The ice velocity field is computed from the dynamical interaction with the atmosphere and ocean. Momentum exchange at the ice-ocean interface is computed from the difference between the top layer ocean velocity and ice velocity. The heat flux is assumed to be proportional to the difference between the surface temperature and the temperature at the freezing point and the friction velocity at the ice-ocean interface. Fresh water fluxes are computed with a constant salinity of 6 psu for sea ice and 0 psu for snow.

The atmosphere and the ocean/sea-ice models exchange information via the OASIS3 coupler (Valcke 2013). The atmosphere model exchanges wind stresses on both water and ice, net precipitation minus evaporation over water and ice, snowfall, evaporation over snow/ice, net shortwave flux, net non-solar heat flux, solar heat flux on ice, non-solar heat flux on ice, and non-solar heat flux derivative. The ocean model exchanges sea surface temperature, sea-ice cover, sea-ice temperature, and sea-ice albedo. A scheme to correct the heat flux from the ocean to the atmosphere is implemented as in Kröger and Kucharski (2011). As noted by Sluka et al. (2016), the main effect of this scheme is the improvement of model climatology and variability in the Eastern tropical Pacific.

2.2 Model simulations and observational data

A set of simulations has been performed to validate the SPEEDY-NEMO model. The model setup and the analysis have been designed to evaluate in particular: (i) the major climatological features of the atmospheric and oceanic circulation, (ii) the surface climate and iii) the leading modes of interannual and multi-decadal variability. A spin-up simulation is run and the model stabilisation is diagnosed via global-mean near-surface air temperature (GSAT), Arctic sea-ice cover and global top-of-atmosphere (TOA) net energy flux. After about 700 years the model fluctuates around a global-mean two-metre air temperature of about 13.9 K and a TOA energy imbalance of about 1.5 W/m^2 (shortwave minus longwave). The imbalance at the top is fairly large but not incompatible with the range of CMIP6 models (Wild 2020). After this spin-up, the model is run for additional 340 years and this simulation is used for analysis and validation of the model performance. The model parameters are those in Kucharski et al. (2016) and the radiative forcing has been specified to be representative of current climate conditions (approx. 1980–2010) through a CO2 optical thickness/absorptivity parameterization. The model integrations are performed with a serial execution of the atmosphere component and a parallel execution of the ocean-ice component with 18 processors. The performance on the coupled model is about 69 days per CPU hour using 18 processors.

The model is validated against a combination of observational datasets and reanalyses. In some cases, depending on the examined variable, multiple datasets are used to account for observational uncertainty. Data from the ERA5 reanalysis (Hersbach et al. 2020) are obtained on a monthly basis from the Copernicus Climate Data Store (Buontempo 2022) for air temperature, zonal wind, precipitation, two-metre temperature, sea surface temperature (SST), height (Z), sea-level pressure (SLP). Reanalysis data of wind and temperature used in Figs. 1, 2 are on the same 8 pressure levels used to interpolate the model output, that is 30, 100, 200, 300, 500, 700, 850 and 925 hPa. The period examined for ERA5 is limited to 1979–2021 to avoid larger uncertainties in the pre-satellite era, but note that in Figs. 5, 6 the period is further reduced to 1979–2014 for consistency with other datasets that cover this shorter time span. Data of meridional wind velocity and temperature have been obtained from the NCEP-NCAR (Kalnay et al. 1996) reanalysis and used in Fig. 4. Gridded observations of sea-ice concentration are obtained from the National Snow and Ice Data Center (Walsh et al. 2019) for the period 1850–2017 and from the Hadley Centre Sea Ice and Sea Surface Temperature (HadISST) dataset (Rayner et al. 2003) for the period 1979–2021. Gridded observed and reconstructed SST are obtained from HadISST for the period 1979–2021 and from the Extended Reconstructed Sea Surface Temperature (ERSST, Huang et al. 2017) dataset. Gridded observation of precipitation from Climate Prediction Center Merged Analysis of Precipitation (CMAP, Xie and Arkin 1997) and from Global Precipitation Climatology Project (GPCP, Adler et al. 2017) for the period 1979–2014 are used. Data from the ORAS4 ocean reanalysis (5 ensemble members, Balmaseda et al. 2013) are used for the period 1958–2012.

2.3 Diagnostics

The global monsoon domain shown in Fig. 5 is computed following Wang et al. (2011) as the area over which the annual range of precipitation is greater than 2.5 mm/day. The annual range of precipitation is defined as the MJJAS minus NDJFM (NDJFM minus MJJAS) precipitation rate in the Northern (Southern) Hemisphere. The eddy heat flux in Fig. 4 is computed as the covariance of daily deviations from monthly means of air temperature and meridional velocity. Sea-ice extent is computed by treating as ice

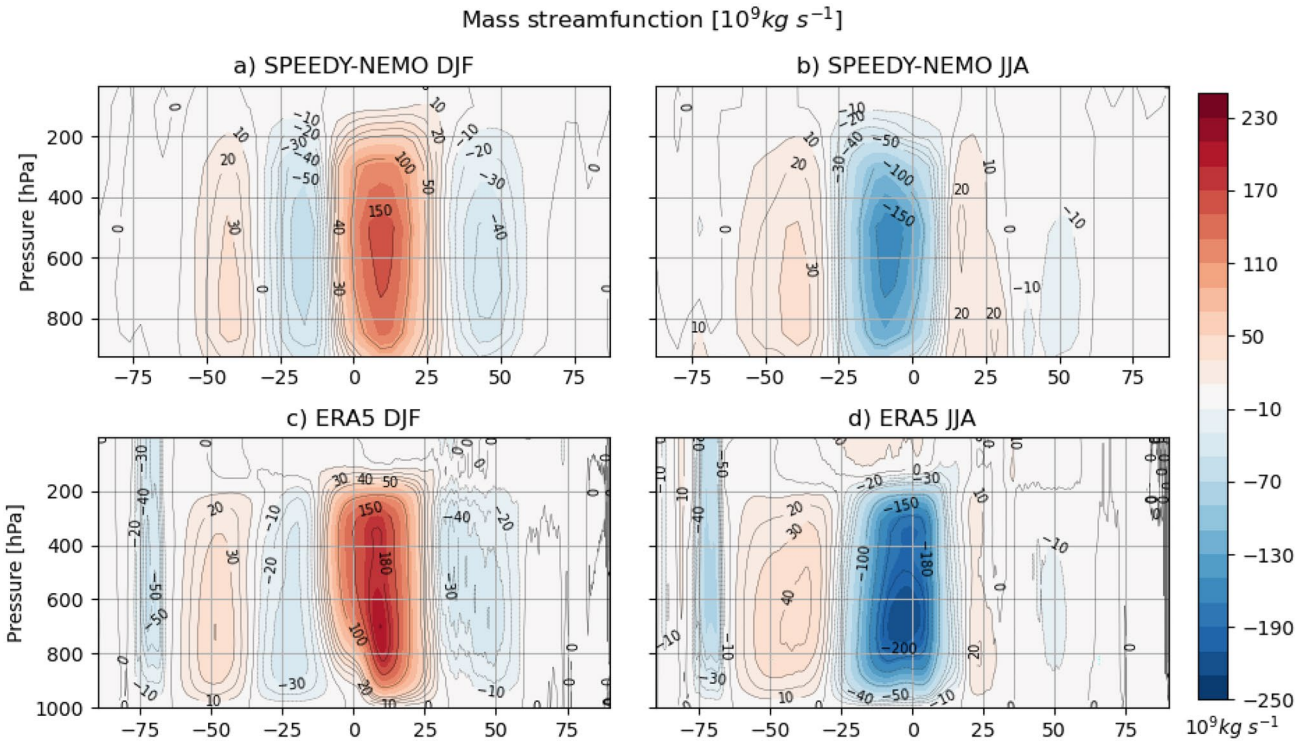

Fig. 1 Climatology of mass streamfunction (10^9 kg s^{-1}) of the zonal mean flow in **a** DJF and **b** JJA for the SPEEDY-NEMO model and **c**, **d** for the ERA5 reanalysis

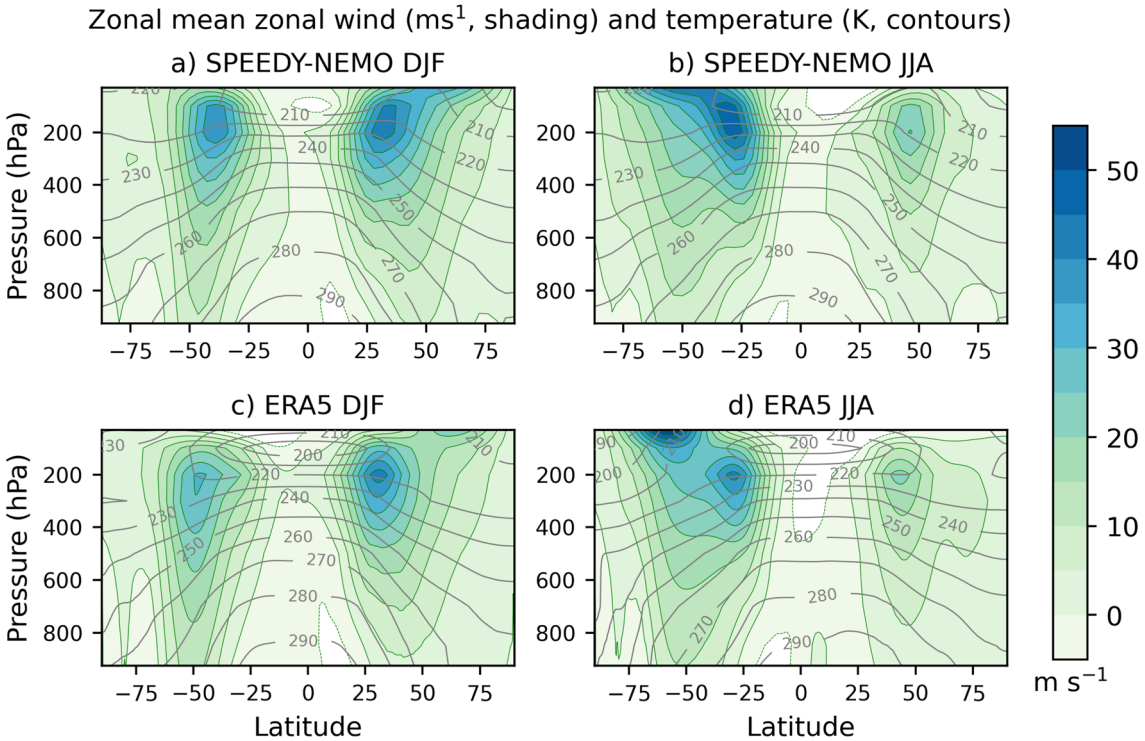

Fig. 2 As in Fig. 1 but for the zonal mean zonal wind in ms^{-1} in shading and contours of zonal mean temperature (drawn every 10 K)

covered all grid points with sea-ice concentration greater than or equal to 0.15. The North Atlantic Oscillation (NAO) index is defined following Hurrel (1995), as the standardized principal component (PC) time-series of the leading EOF of December-February SLP anomalies over the Atlantic sector (20° N–80° N, 90° W–40° E). Similarly, the Southern Annular Mode (SAM) index is defined as the standardized PC time-series of the leading EOF of JJA SLP anomalies south of 20° S (Ho et al. 2012). The Niño3.4 index is defined as the area-weighted average of SST anomalies over 5° S–5° N/170° W–120° W; this index is widely used to define the state of the El Niño-Southern Oscillation (ENSO) also in the context of operational seasonal forecasts (Barnston and Tippett 2013). The Atlantic Multidecadal Variability (AMV) index is computed adopting the definition introduced by Trenberth and Shea (2006), which is the difference between North Atlantic SST anomalies (0–60° N, 0–80° W) and global-mean SST anomalies (60° S–60° N). The Interdecadal Pacific Oscillation is analysed by computing the Tripole Index (TPI) introduced by Henley et al. (2015), which is a linear combination of SST anomalies in three sectors of the Pacific Ocean. The Atlantic Meridional Overturning Circulation (AMOC) is diagnosed with a mass streamfunction computed with the diagnostic package CDFTOOLS (http://meom-group.github.io/doc/CDFTOOLS/) using three-dimensional fields of ocean meridional velocity.

Linear regressions are computed via a least-squares linear fit. The model biases shown in Fig. 8 are computed as the difference between the atmospheric model output minus the corresponding ERA5 field regridded onto the coarser model grid. The regridding operation is performed at constant pressure via bilinear interpolation with the Climate Data Operator (CDO, Schulzweida 2019). Running correlations in Fig. 20 are computed with the Pearson correlation coefficient.

3 Results

3.1 Atmosphere and ocean climatology

The zonal-mean atmospheric circulation is examined in Figs. 1 and 2. Overall, the model error for the latitudinal extent of the cells and their intensity (Fig. 1) is comparable with the range of uncertainty among reanalyses (Nguyen et al. 2013). The latitude of ascending and descending branches are reproduced accurately in the winter hemisphere, while the model slightly misplaces the latitude of the summer cells by about 3–5 degrees. Notably the intensity of the maximum/minimum of the winter Hadley cell is weaker by a factor of about 15%. This indicates a similar bias in the mass flux associated with this cell. The bias is larger in the Antarctic region, where surface biases shown later in the manuscript may play a role. The sign of the surface zonal-mean zonal wind is well reproduced (Fig. 2, shading), with a region of easterly wind in the tropics, a relatively strong westerly wind in midlatitudes and weak easterlies in the polar region. The model correctly simulates the position of local maxima, the subtropical jets of both hemispheres and the stratospheric polar vortex of the cold hemisphere. The intensity of the subtropical jets is overestimated by about 15%. The simulated temperature field shows that the model correctly reproduces the observed vertical gradients and the inversion at the tropopause, as well as a strong seasonality in the stratosphere (Fig. 2, contours). The simulated temperature is flatter in the tropics and shows stronger meridional gradients in the extratropics, which is consistent with the stronger vertical wind shear according to thermal wind balance. The zonally asymmetric component of height at 500 hPa is shown in Fig. 3. This field provides an indication of the ability of the model to reproduce the stationary eddies of the atmosphere, that are zonal asymmetries ultimately driven by topography, land-sea contrast and temperature variations at the sea surface. This field is shown only for the Northern Hemisphere winter, since stationary eddies peak in the cold season and the circulation in the Southern Hemisphere is rather zonally symmetric. It can be seen that the model properly simulates the quasi-wavenumber 2 pattern, with maxima over the eastern North Atlantic and the west coast of North America and minima over the western North Pacific and the Labrador Sea region. Note that the maximum amplitude of the stationary eddies is underestimated in the two centres of action over continental North America. The results in Figs. 1-3 illustrate that SPEEDY-NEMO provides a realistic atmospheric mean flow and a good representation of large-scale wave propagation, that is a desired feature for the purpose of the model as outlined in Section 1.

Figure 4 displays the boreal winter climatological distribution of daily temperature and meridional wind covariance at 850hPa, representative of the sensible heat flux associated with synoptic-scale, transient eddies. Figure 4 suggests that the model correctly identifies the regions of intense baroclinic activity in both the North Atlantic and North Pacific ocean basins, although the magnitude of the sensible heat flux is underestimated in the North Pacific. Interestingly, the model shows secondary maxima in subpolar regions and over Eurasia that resemble observations and are linked to the low-frequency variability of the atmosphere (Ruggieri et al. 2021).

The model reproduces the major large-scale features of precipitation climatology (Fig. 5). Extra-tropical precipitation in the Northern Hemisphere is organised in two major storm-tracks over the ocean basins with local maxima over the oceanic frontal regions (Gulf stream and Kuroshio current; see also Fig. 4). The model climatology over land resembles many observed features,

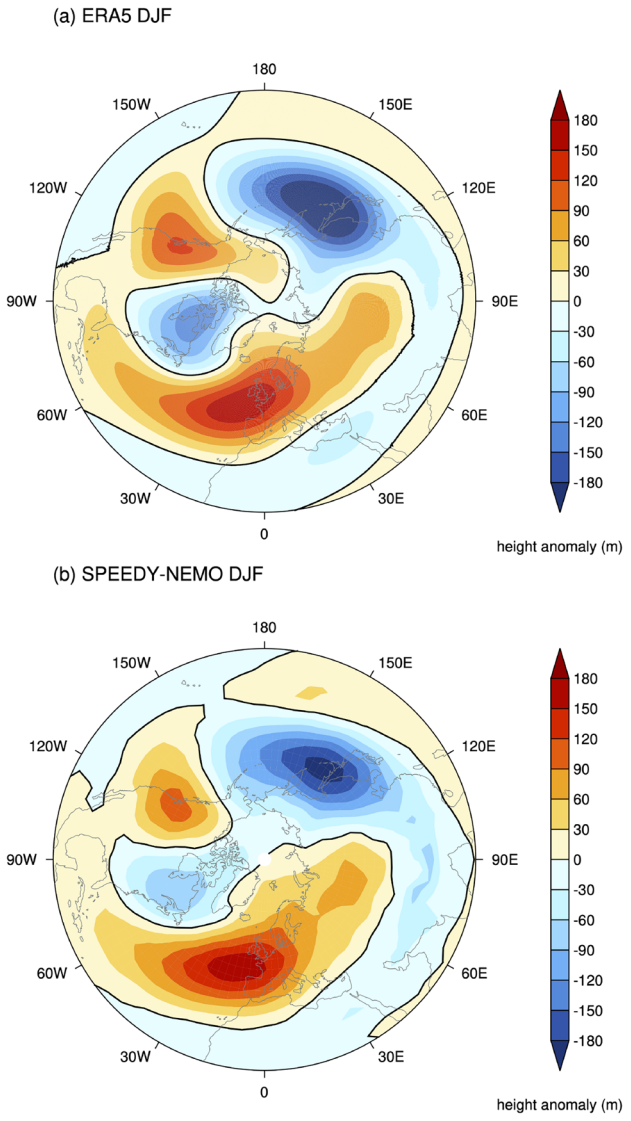

Fig. 3 **a** Height (m) at 500 hPa for DJF after subtracting the zonal mean. This represents the stationary eddy field. Data are from the ERA5 reanalysis. **b** Same as (**a**) for the SPEEDY-NEMO model. The zero line is marked by a black solid contour

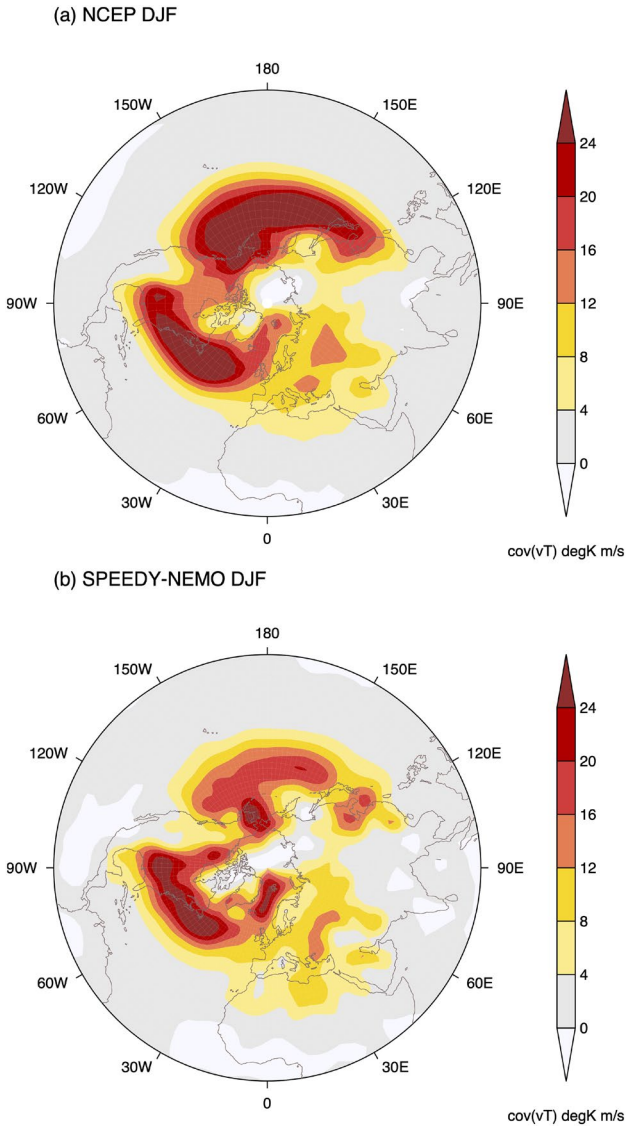

Fig. 4 **a** Mean DJF covariance of daily temperature and meridional velocity anomalies at 850 hPa. Data are from the NCEP/NCAR reanalysis. **b** As in (**a**) but for SPEEDY-NEMO

but notably precipitation is slightly overestimated in winter and substantially overestimated in summer over North America and the Maritime Continent. Longitudinal variations of the ITCZ and their seasonality are correctly simulated. However, Fig. 5 also shows that, at the regional level, the model features substantial biases in the represention of the major global monsoonal systems (Wang and Ding 2008). In the Northern Hemisphere, the South Asian monsoon is poorly represented, with a too low accumulated precipitation while the East Asian monsoon features an overly fragmented pattern (Fig. 5b). The West African monsoon is instead captured, though with spatial and magnitude biases. The North American monsoon is absent over northwestern Mexico and captured only over its southern domain. The model does a relatively better job in the Southern Hemisphere, where all the three regional monsoons are spatially reproduced, although with substantial positive precipitation biases. A more quantitative comparison with observed precipitation can be done with the help of Fig. 6 where the zonal-mean precipitation is shown. Here multiple observational datasets (both reanalysis and gridded observations) are used to account for observational uncertainty. It can be seen that indeed the model quantitatively reproduces the observed profile. In general the modelled precipitation falls within the observational range everywhere except in the Southern Hemisphere equatorial region (Fig. 6a). Here the relative

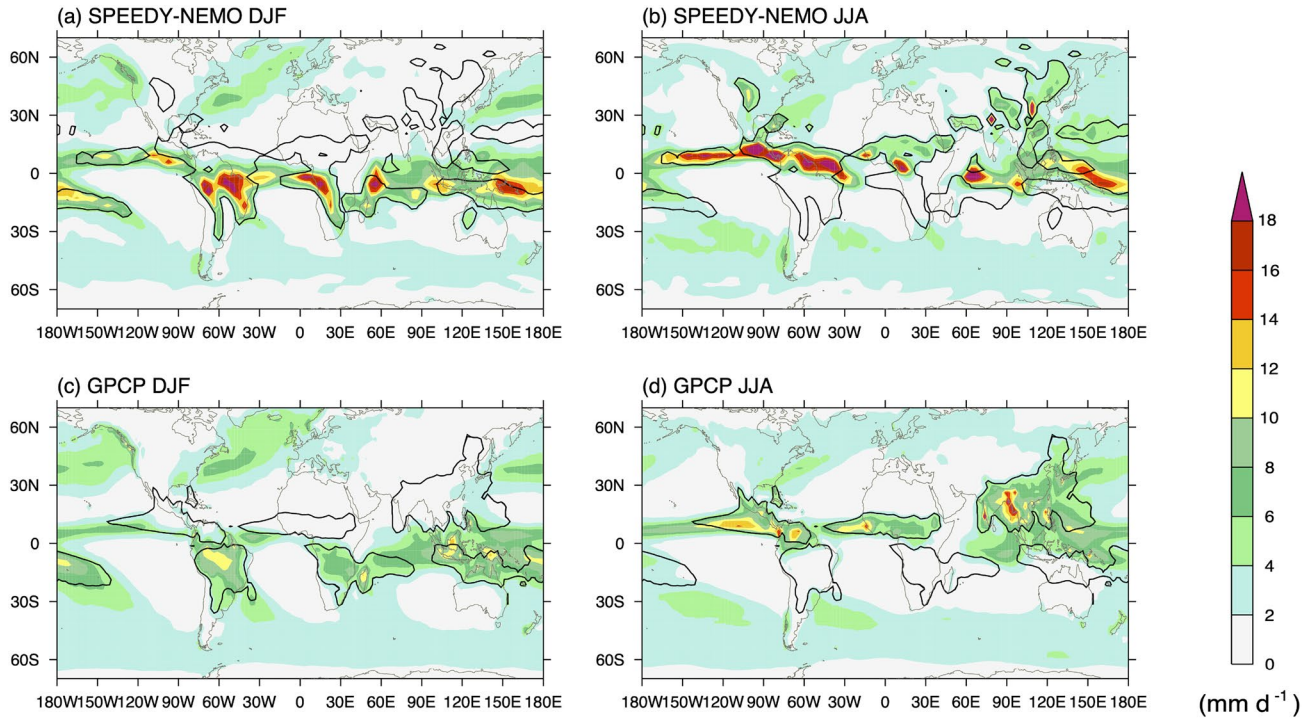

Fig. 5 Climatology of precipitation (mm day^{-1}) in SPEEDY-NEMO for **a** DJF and **b** JJA. The black solid line denotes the global monsoon domain, defined as the area over which the annual range of precipitation – i.e., MJJAS minus NDJFM (NDJFM minus MJJAS) precipitation rate in the Northern (Southern) Hemisphere – is greater than 2.5 mm/day (Wang et al. 2011). **c**, **d** As in (**a**, **b**) but for the GPCP monthly precipitation dataset

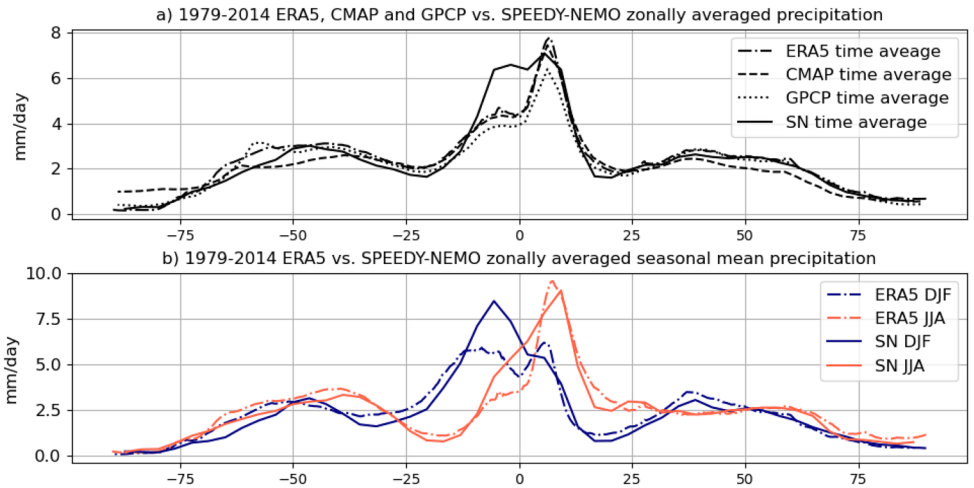

Fig. 6 **a**, **b** Climatology of zonal mean annual mean precipitation in units of mm day^{-1} in the SPEEDY-NEMO model (solid line), the ERA5 reanalysis (dashed-dotted line), the CMAP (dashed line) and GPCP (dotted line) gridded observations. **b** Climatology of zonal mean total precipitation in units mm day^{-1} in DJF (blue lines) and JJA (red lines) for the SPEEDY-NEMO model (solid lines) and the ERA5 reanalysis (dashed-dotted lines)

error is about 45%, corresponding to a positive bias of the order of 2 mm day^{-1}. This is not surprising, given the similar bias reported in many climate models of different complexity, including state-of-the-art (Blaker et al. 2021). A much smaller model bias, negative in this case, can be identified in the subtropical regions. The seasonal cycle of the zonal-mean precipitation is also well reproduced (Fig. 6b), in particular the latitudinal migrations of local maxima and minima are accurately modelled.

The two-metre air temperature climatology (Supplementary Material, Fig. S1) and SST climatology (Fig. 7) show that the model captures regional features of the observed field, particularly over ocean - the longitudinal gradients in the tropics and the sharp, meridional gradients in the extra-tropics, such as the Gulf Stream in the North Atlantic and the Kuroshio-Oyashio extension in the North Pacific. Over land and at high latitudes, the model underestimates cold conditions during boreal winter and warm conditions during

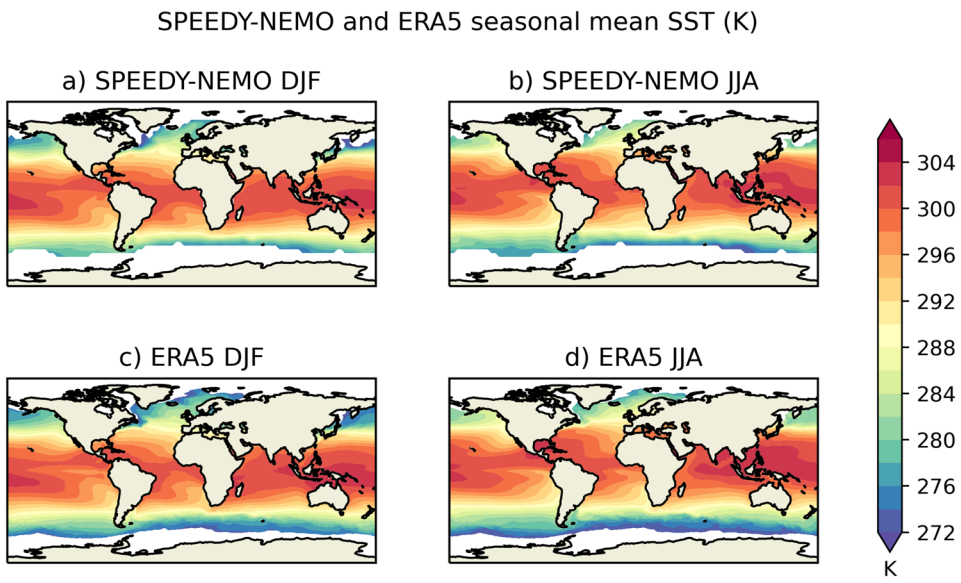

Fig. 7 Climatology of sea surface temperature (K) in **a** DJF and **b** JJA for the SPEEDY-NEMO model and the **c**, **d** the ERA5 reanalysis

boreal summer. Figure 8 shows the model bias of the zonal mean temperature and zonal wind. The zonal wind bias is larger in the Southern Hemisphere and in the upper troposphere. The positive bias in the mid-latitude upper-troposphere is in thermal wind balance a colder mid troposphere. A useful comparison with state-of-art GCMs is given by (Moreno-Chamarro et al. (2022), Fig. 6). The bias in the stratospheric temperature is also noticeable, it is common to the atmosphere only model documented in Molteni (2003) and attributable to dissipative terms applied at the stratospheric level and to empirical treatment of radiative processes. The bias of the SPEEDY-NEMO model zonal mean zonal wind is broadly comparable with that of high-resolution coupled models. In particular, in the mid-lower troposphere of the Northern Hemisphere the bias is notably small. A term of comparison for the order of magnitude of zonal mean temperature bias is given by Semmler et al. (2020). The 2D zonal wind bias in Fig. 8b is useful to confirm that in general the relatively small bias found in the zonal mean is not explained by larger compensating errors. Finally the SST bias reveals a worse performance of the model in subpolar regions and in the Southern Atlantic ocean, but the bias is otherwise confined to values in the range of ± 1 K (Fig. 8c).

Figure 9 shows sea-ice concentration (SIC) and extent (SIE) in the polar and subpolar regions of the two hemispheres. March and September have been selected as they roughly correspond to the maximum and minimum, respectively, sea-ice cover in the Arctic both in models and observations; vice versa for the Antarctic. Winter SIE in the Arctic is accurately reproduced by SPEEDY-NEMO (Fig. 9a,e), and similarly winter SIC is reasonably modelled in several marginal seas of the Arctic, such as the Bering and Labrador Seas. In September (Fig. 9b,f), while the model correctly simulates the retreat of sea ice into high latitudes, it overestimates SIC along the Siberian coast and over the Barents-Kara Seas. This can be partially explained by the pronounced declining trend of summer Arctic sea-ice cover (see also Fig. 9) that is robustly attributed to external forcing (e.g., Smith et al. 2008) and is not accounted for in the model setup since radiative forcing is kept fixed. In the Antarctic (Fig. 9c–h), the seasonal range of sea-ice cover is again reasonably well simulated by the model, with the clear exception of the Weddell and Ross Seas, probably linked to the lack of ice-shelf dynamics characteristic of these areas. Antarctic SIC is overall underestimated. In Fig. 10 we show the time series of the NSDIC observed Arctic sea ice extent in late winter and summer (JFM and JAS) and the corresponding seasonal climatology and interannual variability in SPEEDY-NEMO. This analysis confirms that the model is able to reproduce a realistic value of ice extent although the interannual variability is slightly exaggerated.

Finally, some aspects of sub-surface ocean circulation are presented. Figure 11 shows the climatology (contours) and variability (shading) of the Atlantic meridional overturning circulation (AMOC) in SPEEDY-NEMO as compared to reanalysis (ORAS4). The model properly simulates the meridional and vertical extent of the climatological AMOC, as well as its relative maximum at northern mid-latitudes, although the strength is slightly underestimated. It also captures the position (45° N) and depth (2000 m) of the variance peak, but its amplitude is approximately half of that in reanalysis. Figure 12 displays the modelled and observational climatology (contours) of the thermocline, which is shown in the equatorial Pacific and equatorial Atlantic during the corresponding seasonal maximum of the cold tongue development and SST variability, namely in boreal winter (DJF) and summer (JJA) respectively. Interannual variability of ocean temperature is also displayed (shading).

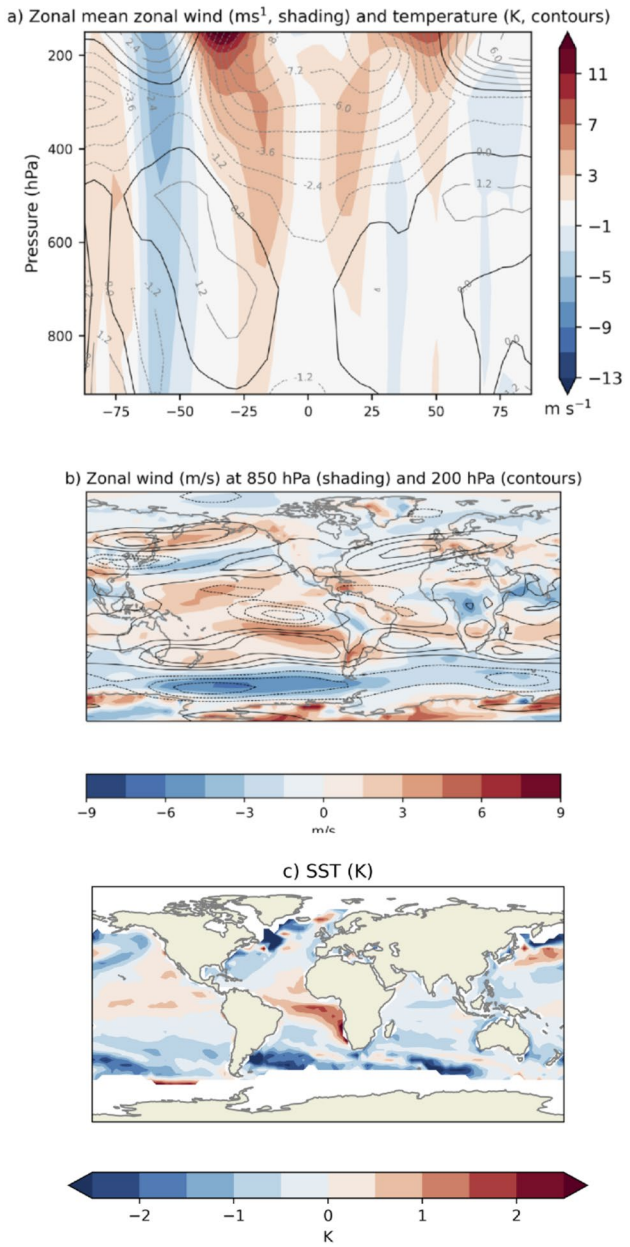

Fig. 8 Annual mean model bias with respect the ERA5 climatology of **a** zonal mean temperature (contours drawn every 1.2 K) and zonal wind (shading, m/s); **b** zonal wind at 850 hPa (shading, m/s) and 200 hPa (contours drawn every 3 m/s); (**c**) and sea surface temperature

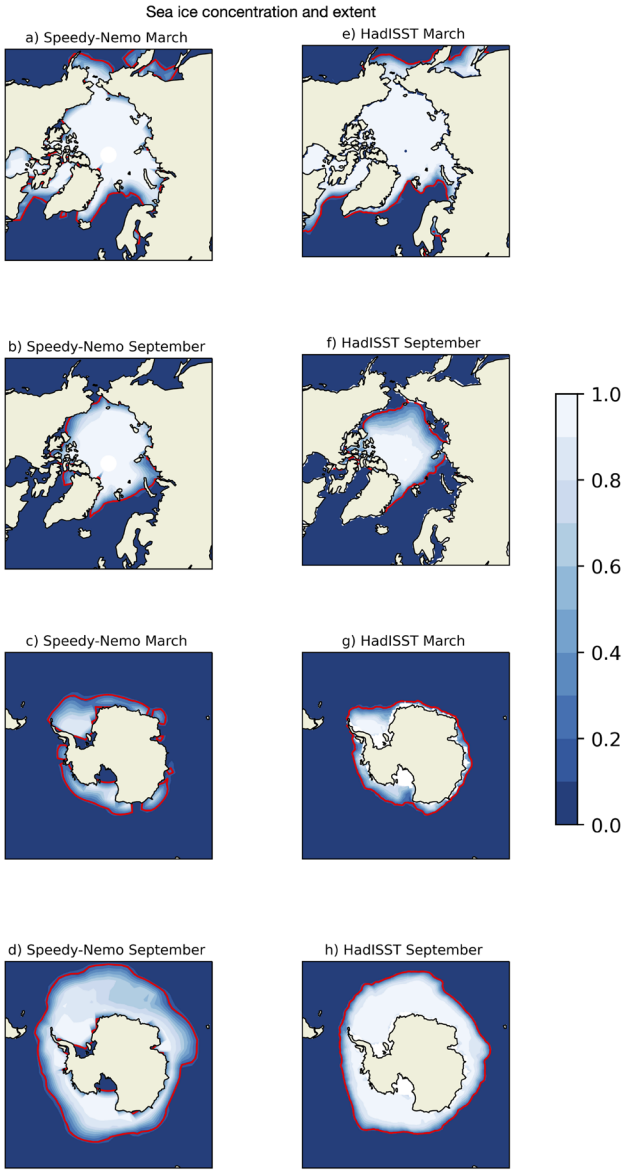

Fig. 9 Climatology of March and September sea ice concentration (shading) and extent (red contour) for **a**–**d** the Speedy-Nemo model and **e**–**h** HadISST in both hemispheres

SPEEDY-NEMO correctly simulates the slope of the thermocline in both ocean basins. The variability around the thermocline is weakly biased over the Atlantic but largely underestimated over the Pacific.

3.2 Climate variability modes

The low-frequency variability of the atmosphere is examined by looking at the North Atlantic Oscillation (NAO) and Southern Annular Mode (SAM). Figure 13 shows the regression map of SLP anomalies onto the corresponding principal component based on SLP in boreal winter (DJF) and austral winter (JJA), respectively (see Sect. 2.3 for details). In the Northern Hemisphere (Fig. 13a,c), SPEEDY-NEMO broadly simulates the large-scale structure of the NAO but with a clear lack of variance at polar latitudes, which might include effects of a poorly-resolved stratosphere as discussed by García-Serrano and Haarsma (2017). The comparison with the NAO pattern of the atmosphere only model suggests that the ocean coupling is slightly detrimental for the representation of this mode of variability in this model. On

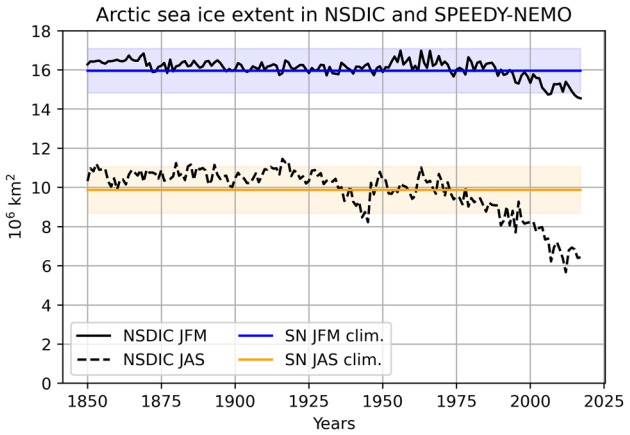

Fig. 10 Time series of seasonal mean NSDIC Arctic sea ice extent in JFM (km^2, solid black line) and JAS (dashed black line. The corresponding seasonal climatological values for Speedy-Nemo are shown with a blue (JFM) and a yellow (JAS) horizontal line. The coloured shading indicates the area between ± one standard deviation computed over the time series of seasonal means (interannual variability)

a finer scale, the model exhibits errors in the representation of the NAO that are well-documented and common to more complex and higher-resolution models. More specifically, long-lasting biases in magnitude of the NAO regressions are documented for three generations of coupled GCMs (Fasullo et al. 2020). Also, the overestimated signal in the North Pacific is documented (Osborn et al. 1999) and endemic in climate models (Gong et al. 2016). In the Southern Hemisphere (Fig. 13b,d), SPEEDY-NEMO rightly captures the meridional structure of the SAM between middle and high latitudes, although it overestimates the zonal extension of the Pacific's centre of action and underestimates the amplitude of the Indian's centre of action.

In the following, two major modes of interannual SST variability are analysed. The SST signature of El Niño-Southern Oscillation (ENSO, Fig. 14) during its mature phase, namely in boreal winter (DJF), is rather consistent with observations, with anomalies of about 0.5–1 K in the equatorial Pacific, a dipole of about 0.3 K in the Indian Ocean and Maritime Continent, and a signal in the extra-tropical North Pacific. The ENSO atmospheric teleconnections are diagnosed in Fig. 15 by regressing height in the upper troposphere (200hPa; contours) and precipitation (shading) onto the Niño3.4 index. In agreement with atmosphere-only simulations prescribing observed SSTs (Kucharski et al. 2013), here in coupled mode, the model reproduces the ENSO atmospheric response in both the tropics and extra-tropics of the two hemispheres. The signal in the North Pacific-American sector is particularly close to observations, whereas a signal in western Eurasia appears spurious or misplaced. It is important to remark that while many features of the ENSO teleconnections are robustly assessed in literature, the impact over Europe and Eurasia is still largely debated (e.g., Mezzina et al. 2023, and references therein). Deviations from the observed precipitation pattern in the tropics could be explained by the model error in reproducing large-scale convective patterns in the over the maritime continent. The monthly interannual standard deviation (Fig. 16a) shows that the simulated variability is too low in winter and too high in summer (about 15%), resulting in a flat annual cycle. This is disappointing given the purpose of the model, but it is a common signature of CMIP5 models (McKenna et al. 2020; Chen and Jin 2021) that is modified but not clearly improved in the CMIP6 generation. The power spectrum (Fig. 16b) shows that the simulated variability lies in the 3–10 year range, with an excessive load on specific bands (4 and 7 years), a behaviour that can be even

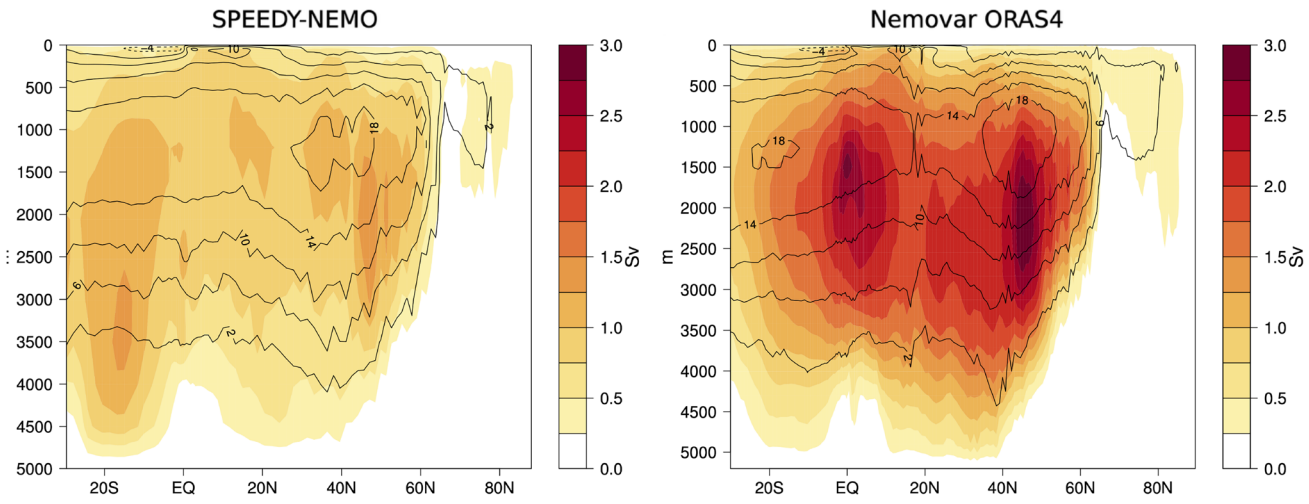

Fig. 11 The Atlantic meridional overturning circulation (AMOC): climatology (contours, drawn every 0.4 Sv) and variability (shading) of the AMOC streamfunction, based on annual means, for SPEEDY-NEMO (left) and the 5-member ensemble Nemovar ORAS4 reanalysis (right)

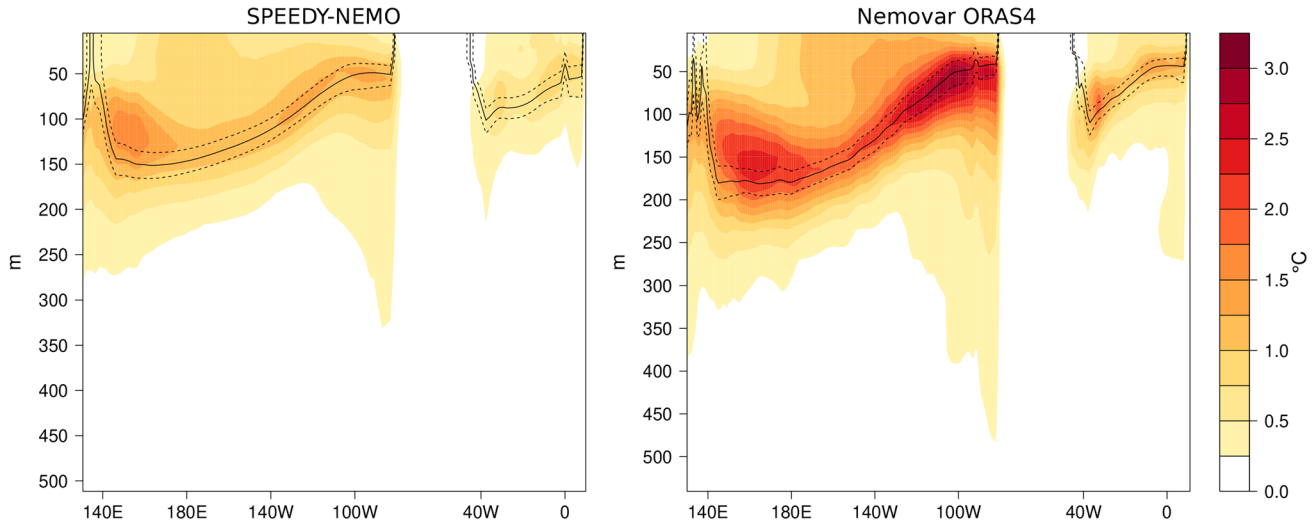

Fig. 12 Climatology of the thermocline depth (contours), estimated as the 20° C isotherm (solid) - surrounded by 18° C and 22° C (dashed) - averaged over 3° S–3° N in the equatorial Pacific during winter (DJF) and equatorial Atlantic during summer (JJ), for SPEEDY-NEMO (left) and the 5-member ensemble Nemovar ORAS4 reanalysis (right). Interannual variability of ocean temperature is also shown (shading)

exacerbated in state-of-the art models (Yang et al. 2019). Still at interannual time-scales, Fig. 17 shows the spatial pattern of the leading mode of SST variability in the tropical Atlantic, i.e. the Atlantic Niño, computed as regression map onto the ATL3 index (Zebiak 1993) in June-July. Following the correct simulation of the regional sub-surface climatology (Fig. 12), SPEEDY-NEMO is able to capture the anomalous tongue in the equatorial Atlantic, but overestimates the opposite-sign anomalies surrounding it.

In Fig. 18 two major modes of decadal variabilty are analysed, namely the Atlantic Multidecadal Variability (AMV) and the Interdecadal Pacific Oscillation (IPO). The standard deviation of the model AMV index is about 0.09K which is broadly in agreement with observational estimates (0.12 K for HadISST and 0.10 for ERSST; see also Fig. 3 in Mavilia et al. (2018) for a comparison with CMIP5 models). The agreement in terms of AMV amplitude is also confirmed in Fig. 18a and c, where the model reproduces the horseshoe-like pattern with a local maximum in the subpolar region. The secondary maximum in the Labrador Sea-Fram Strait area (arguably linked to AMV-induced sea-ice variability, see Castruccio et al. (2019)) is also reasonably modelled by SPEEDY-NEMO. The model also features La Niña-like conditions in the Tropical Pacific, which is less clear in observations where the relationship depends on the exact definition of the index and the examined period (not shown), but was demonstrated to be a plausible teleconnection of the AMV (see e.g. Ruggieri et al. 2021, and references therein). The power spectrum of the modelled AMV index (not shown) resembles that from observations at relatively high frequency, where the model correctly simulates a spectral peak at 25–30 years (see also Mavilia et al. 2018; Ba et al. 2014). The model shows variance at very low frequency, less than 100 years^{-1}, which is common to other coupled GCMs (Mavilia et al. 2018). In this case the comparison with observations is hampered by the limited length of the time series. To examine the multi-decadal variability in the Pacific Ocean Fig. 18 depicts the regression of SST onto the Tripole index (TPI). The TPI index was introduced by Henley et al. (2015) to facilitate the comparison of the Interdecadal Pacific Oscillation between models and observations. The IPO is characterised by a tripole of SST anomalies in the Pacific, in both hemispheres and at tropical and extra-tropical latitudes (see Fig. 18d). Figure 18b shows that SPEEDY-NEMO reproduces this mode of variability and the agreement with observations is substantial. The standard deviation of the TPI index in the model is about 0.35 K, whereas the corresponding value in ERSST is about 0.42 K.

4 Potential applications and added value

Results presented in the previous sections point at SPEEDY-NEMO as a suitable modelling tool to investigate variability modes on S2D time-scales that involve atmosphere and ocean dynamics and/or ocean–atmosphere coupling. Likewise, this model framework is appropriate to explore different aspects of the variability in the climate system. The suggested applications of the model are broadly aligned to the recommendations of Balaji (2021). Two examples analysing climate instability and non-stationarity follow.

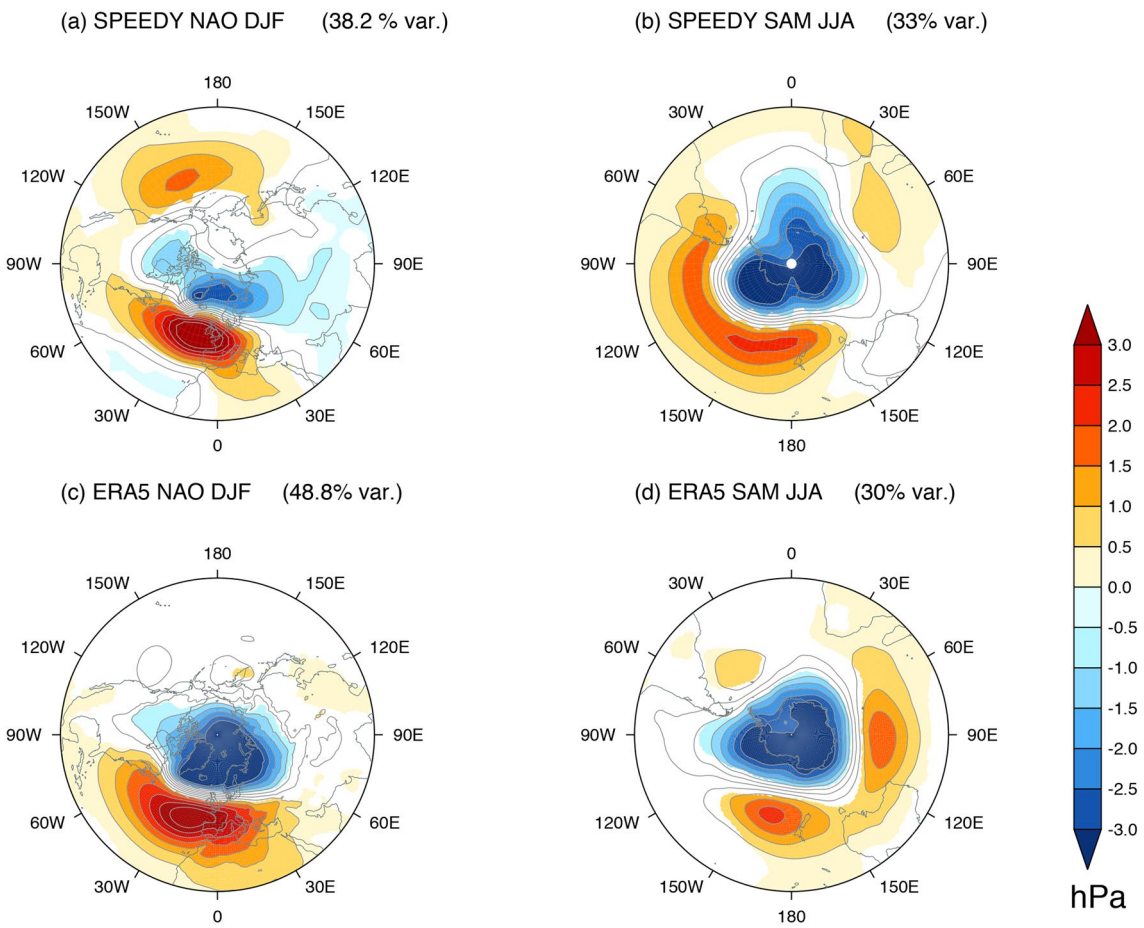

Fig. 13 **a** The DJF NAO pattern as represented in SPEEDY-NEMO by the linear regression of the standardized first PC of the DJF mean sea level pressure seasonal anomalies over the Atlantic sector (20–80N, 90W–40E) onto the same field. **b** The SAM during JJA as the linear regression of the standardized first PC of the JJA mean sea level pressure anomalies south of 20 S onto the same field. **c**, **d** as in (**a**), (**b**) but for the ERA5 reanalyses. Color shading is shown only where the linear regression is statistically significant at the 5%. The percent numbers indicate the fraction of variance explained by the first PC

Figure 19a shows the sea-ice cover averaged over a region corresponding to marginal seas bounding the Antarctic continent (roughly coinciding with the Weddel Sea, the Lazarev Sea, the Riiser-Larsen Sea and the Cosmonauts Sea). By comparing the time series computed with SPEEDY-NEMO and the climatology and variability in HadISST, it can be seen that the model simulates a realistic albeit slightly underestimated sea-ice cover in this region. The model yields an abrupt transition towards a state with reduced sea-ice that persists for several decades. The system then reverts back to the previous state with another abrupt transition. This kind of behaviour in Antarctic sea-ice was found in simulations with high-end models and fixed radiative forcing by Drijfhout et al. (2013) and Drijfhout et al. (2015). It is arguably a potential tipping point of the climate system (Armstrong McKay et al. 2022). SPEEDY-NEMO could be a piece of a hierarchy of models to study this and other abrupt changes and test the sensitivity and robustness to model physics formulation.

Another interesting example is given by the potential non-stationarity of the AMV-AMOC relationship. This is the case of a phenomenon that cannot be easily constrained by observations due to shortness of records and partial inadequacy of observational proxies, but can be addressed with a hierarchy of numerical models of different complexity. In the SPEEDY-NEMO run analysed here, the correlation between the AMV index and the intensity of the AMOC (diagnosed with mean value of the streamfunction between 25° N–50° N and 500−1.500 m, as in Bellucci et al. (2022)) is about 0.59. Figure 20a shows the running correlation between the AMOC and the AMV time series computed with a running window of 80 years. Here we can see a drop of the correlation that reaches a minimum at about year 90 of analysis. A positive correlation is then recovered after 100 years, reaching values of about 0.9 that persists until the end of

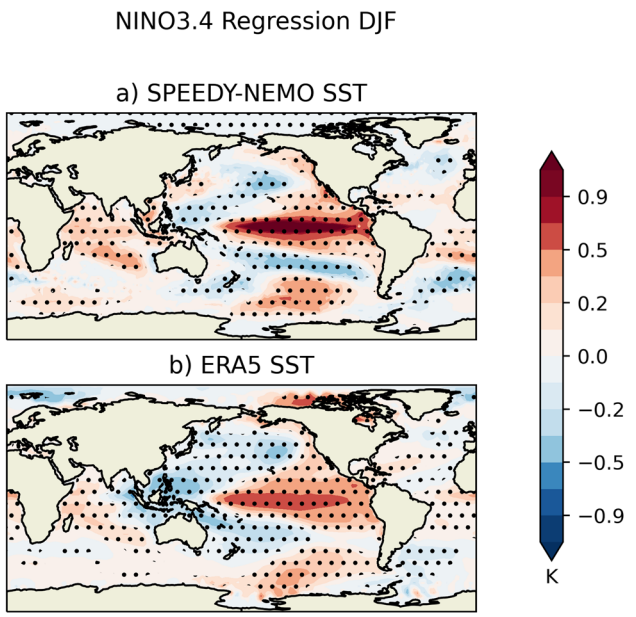

Fig. 14 Linear regression coefficients onto the standardized Niño3.4 index of sea surface temperature (K) for **a** SPEEDY-NEMO and **b** ERA5. Stippling indicates region with statistically significant correlation at the 99% confidence level

the simulation. The behaviour of the running correlation can be better understood by looking at the corresponding low-pass filtered time series in Fig. 20b. Here it can be seen that the first part of the run features small-amplitude and fast oscillations with the AMV and AMOC mostly out of phase. The second part of the run shows instead larger and more persistent excursions of the AMOC that are closely encompassed by the AMV. The different amplitudes can be quantified by the running standard deviation displayed in Fig. 20c that essentially confirms a larger variability in second part of the time series. The episode of non-stationarity in the AMV-AMOC relationship found in SPEEDY-NEMO is fully consistent with the picture given by CMIP6 models, recently documented by Bellucci et al. (2022). SPEEDY-NEMO could be exploited to produce large sampling of AMV-AMOC decorrelation events in order to better understand the underlying dynamics or to study how perturbed parameters in the model formulation can affect this non-stationary relationship.

As outlined by Merryfield et al. (2020), climate prediction models are still affected by non-negligible errors in representing predictable teleconnections that are fundamental for forecast skill over land. A consequence of this is that often hybrid statistical-dynamical forecasts are employed to exploit predictable signals (see e.g., Dobrynin et al. 2022), with all the complications and drawbacks that affect forecasts based on statistical models. While it is arguably overambitious to imagine that SPEEDY-NEMO can be used to guide the reduction of bias in high-end models, intermediate-complexity models like SPEEDY-NEMO can provide guidance in understanding the consequence of model biases for climate predictions. A recent example based on the atmosphere model SPEEDY is given by Di Carlo et al. (2022), where a large set of simulations were performed to study the dependence of the extra-tropical ENSO teleconnection on the model bias in the North Pacific atmospheric circulation. They corroborated and expanded the conclusions reached by similar studies with high-end models (Tyrrell and Karpechko 2021; Benassi et al. 2022) and outlined how

Fig. 15 As in Fig. 14 but for precipitation (**a**–**c**, mm day^{-1}) and geopotential height at 200 hPa (**b**–**d**, m)

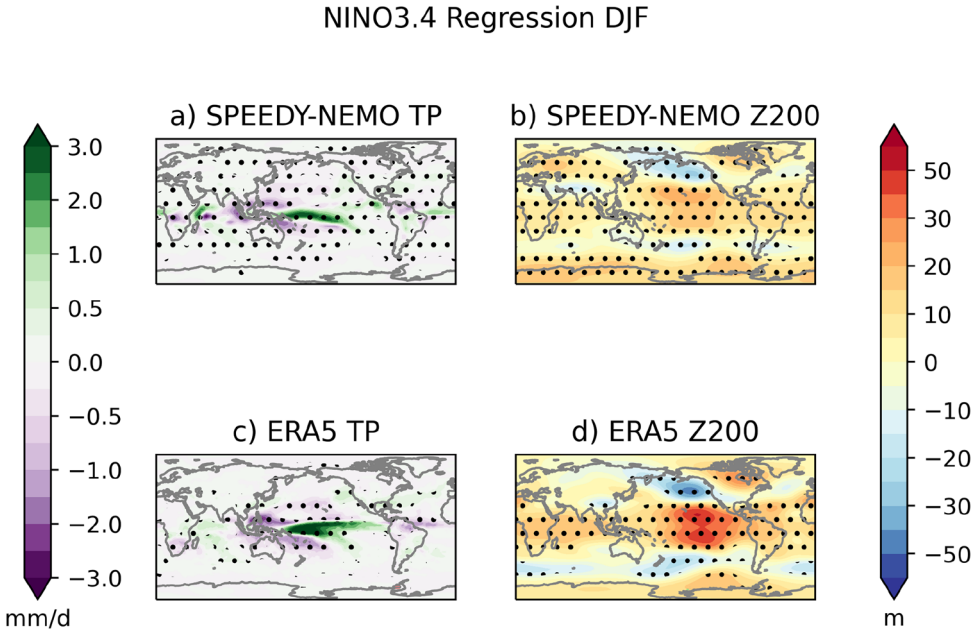

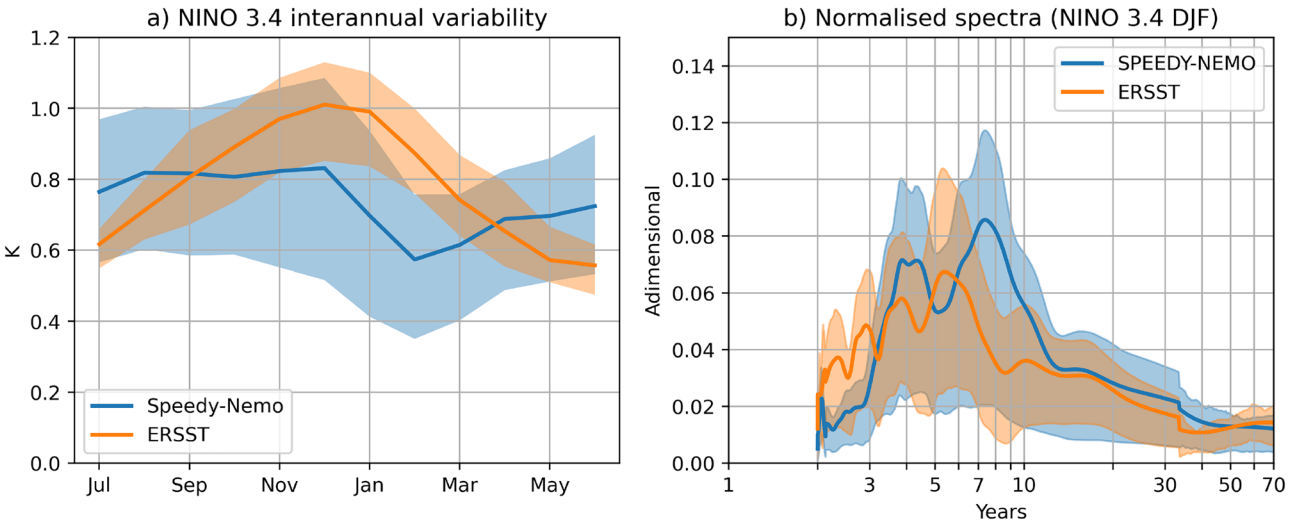

Fig. 16 **a** Interannual standard deviation of the monthly mean Niño3.4 index for SPEEDY-NEMO (blue) and the ERSST (orange). **b** As in (**a**) but for the normalised spectra. The solid line and the shading show respectively the median and the interquartile range of a distribution obtained by subsampling time series of 50 years

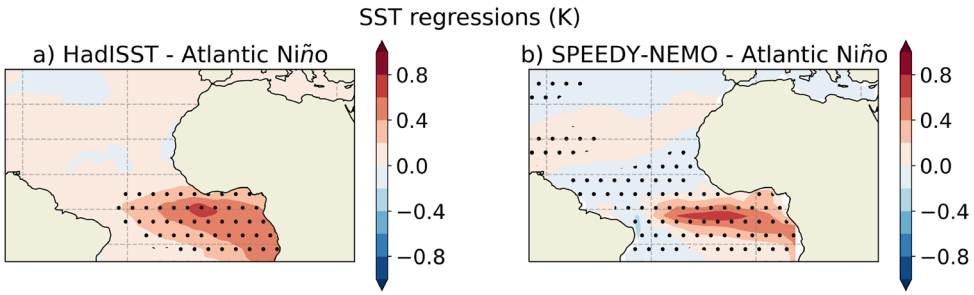

Fig. 17 Sea surface temperature regression onto the standardised ATL3 index in June-July, respectively for SPEEDY-NEMO (right) and HadISST (left). Stippling indicates region with statistically significant correlation at the 99% confidence level

ENSO-related temperature and precipitation signals over land are affected by errors in the model mean-climate. With SPEEDY-NEMO, this approach could be extended and generalised to oceanic and coupled processes, a research avenue that, probably, has not been widely explored so far.

This approach can arguably be of uttermost relevance to tackle the signal-to-noise paradox, a major issue in S2D predictions that de facto limits the estimate of predictability and affects negatively raw dynamical predictions (Smith et al. 2020). The signal-to-noise paradox is indeed an elegant example of a crucial issue in S2D climate prediction that affects the forecast skill of state-of-art models (Scaife and Smith 2018) and is reproducible even in low-complexity models such as the Lorenz63 system (Mayer et al. 2021). The analysis of the autocorrelation of the NAO index (not shown) in the run presented in this study reveals that, if the hypotheses introduced by Zhang et al. (2021) hold, then SPEEDY-NEMO should not be affected by the signal-to-noise paradox described by Scaife and Smith (2018). This is a speculative but intriguing indication that the model may not reproduce the paradox in the presented sets. Sets of retrospective forecasts with SPEEDY-NEMO could be used to diagnose how the signal-to-noise ratio is affected by perturbations in the model formulation (for instance surface parameterisations and atmospheric resolution) and by model initialisation and ensemble-generation techniques. It is not unrealistic to hypothesize a modelling tool based on SPEEDY-NEMO, that can generate sets of large-ensemble hindcasts with different combinations of model formulation and initialisation techniques, to further evaluate properties of the forecast quality (e.g., skill and signal-to-noise metrics). The DYNCAST and OCEANIDE projects in seasonal prediction, relying on results by Mezzina et al. (2020), and the BONSAI (https://www.ecmwf.int/en/research/special-projects/spitbeal-2022) and TBI-MULMOD (https://www.csic.es/en/node/2058253) projects in decadal prediction are examples of ongoing activities working in this direction with SPEEDY-NEMO.

Along these lines, climate predictions based on SPEEDY-NEMO can be a training field to explore developments in data assimilation (Tondeur et al. 2020), as the model already supports data assimilation schemes. Last but not least, this

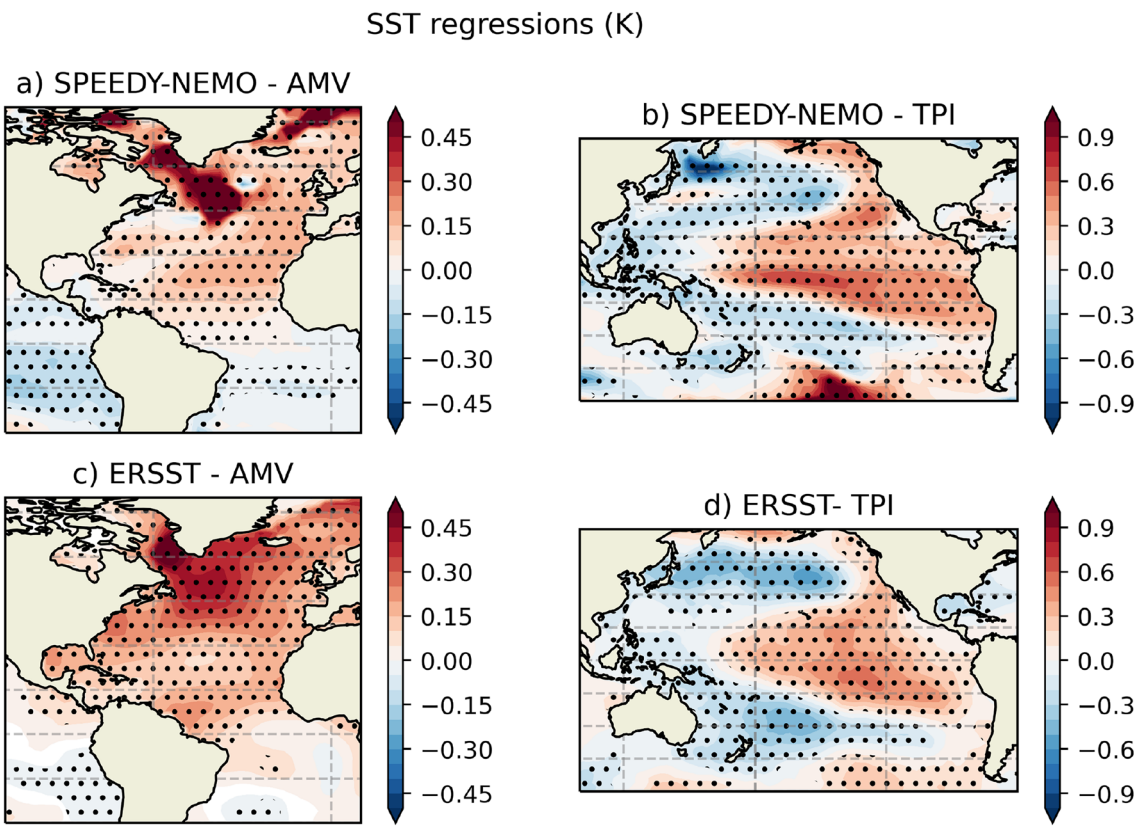

Fig. 18 Linear regression coefficients (K) of sea surface temperature onto **a**, **c** the standardised AMV index and **b**, **d** the standardised TPI index for the **a**, **b** SPEEDY-NEMO model and **c**, **d** the ERSST dataset. Stippling indicates region with statistically significant correlation at the 99% confidence level

kind of intermediate-complexity coupled models can foster innovation in the model code and algorithms that is fundamental to adjust our modelling tools to future hardware architectures. Low precision components (Lang et al. 2021), on-the-run diagnostic routines and stochastic and/or data-driven parameterisations (Ross et al. 2022) can be effectively tested in a simplified modelling suite such as SPEEDY-NEMO.

5 Concluding remarks

This manuscript reports the climatology and variability of a coupled general circulation model: SPEEDY-NEMO. This climate model complements other models in the SPEEDY family of which it is the only member with a fully-coupled primitive-equation ocean, complementing previously documented models where SPEEDY was coupled to regional ocean models (Haarsma et al. 2005; Bracco et al. 2005, 2007). The presented version features a fairly low horizontal and vertical resolution (3.7°/8 levels in the atmosphere; 2°/31 levels in the ocean) and a full spectrum of simplified physical parameterisations.

The modelled atmospheric circulation and surface climate (including sea-ice cover and sea surface temperature) documented in this study are quantitatively in agreement with reanalysis data, with systematic errors comparable to observational uncertainty and biases of CMIP5 and CMIP6 models. Major exceptions in this respect are found in the surface temperature of polar and subpolar regions and in seasonal variations of precipitation over monsoonal areas. Presented results show that the model underestimates transient eddy fluxes in the atmosphere but reproduces realistically the low-frequency variability of the atmosphere and the leading modes of large-scale interannual and decadal variability in the ocean. These findings suggest that the model can be used to produce meaningful low-resolution climate predictions on seasonal-to-decadal time-scales and to perform targeted sensitivity experiments that can support and inform the development of operational forecasts.

Based on the presented results, we argue that SPEEDY-NEMO can be instrumental in operationalising the hierarchical approach advocated by Held (2005) in the field of near-term climate prediction. We have put forward a range of scientific questions that could be investigated using SPEEDY-NEMO as intermediate-complexity element of

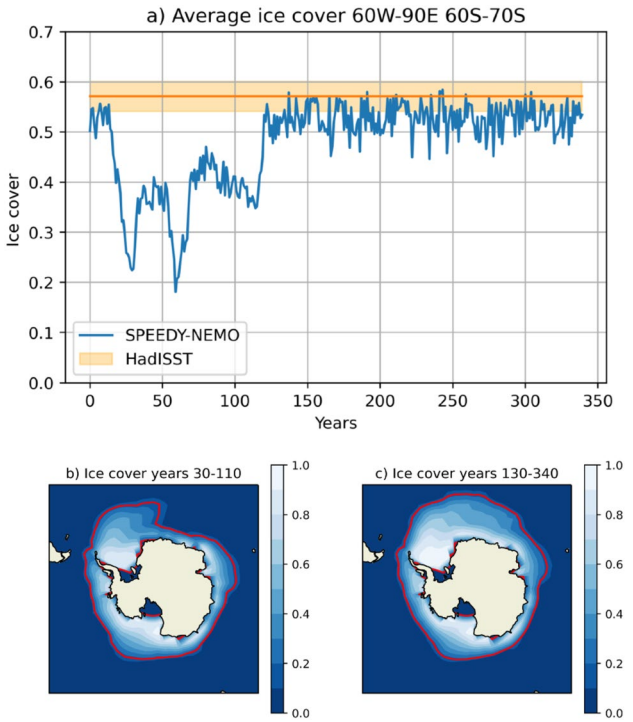

Fig. 19 **a** The blue solid line is the average annual ice cover in the sector 60W–90E 60 S–70 S simulated by SPEEDY-NEMO. The horizontal line and the shading indicate respectively the corresponding mean and one standard deviation range for the HadISST. **b** and **c** show the sea ice concentration (shading) and extent (red contour) averaged respectively in years 30–110 and in years 130–340

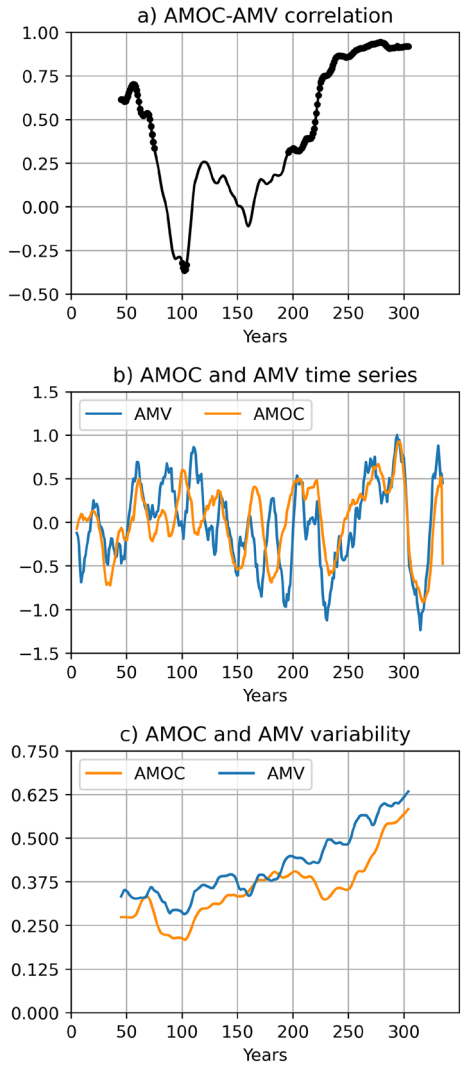

Fig. 20 Non-stationarity of the AMOC-AMV relationship in SPEEDY-NEMO. **a** Running correlation between the AMV and the AMOC time series with a running window of 80 years. Dots indicate statistically significant correlations at the 99% confidence level. **b** Standardized time series of the AMV (blue) and AMOC (yellow). **c** Running standard deviation of the AMV (blue) and AMOC (yellow) with a running window of 80 years

such a model hierarchy. More specifically, we suggest that phenomena of S2D climate variability, which are often investigated in idealised setups, could be studied with SPEEDY-NEMO by producing sets of long simulations and/or large-ensemble hindcasts over the past decades. Further development with a relatively small effort may lead to a flexible modelling tool to comprehensively assess climate variability, predictability, prediction and change with large enough sampling to test robustness.

Finally, the model can also represent a training environment for proof-of-concepts of ensemble generation and initialisation techniques that nowadays are arguably at their infancy in the operational context.

Supplementary Information The online version contains supplementary material available at https://doi.org/10.1007/s00382-023-07097-8.

Acknowledgements The authors are grateful to two anonymous reviewers for constructive comments on the first version of the manuscript. PR is grateful to Alessio Bellucci for helpful discussions on an early version of the manuscript. PR and CG acknowledge the use of computational resources from the parallel computing cluster of the Open Physics Hub (https://site.unibo.it/openphysicshub/en) at the Department of Physics and Astronomy of the University of Bologna. JG-S acknowledges funding from the Spanish DYNCAST project (CNS2022-135312). DV was supported by the "María Zambrano" programme (OCEANIDE project).

Author contributions PR designed the study and wrote the original paper draft. JGS and FK contributed to the writing of the submitted manuscript. CG performed the numerical simulations. PR, SP, CG, DV and AA contributed to the analyses. All authors discussed the results and contributed with manuscript revisions.

Funding Open access funding provided by Alma Mater Studiorum - Università di Bologna within the CRUI-CARE Agreement. The authors declare that no funds, grants, or other support were received during the preparation of this manuscript.

Data availability Data used in the study are made available upon request to the corresponding author via the Open Physics Hub (https://site.unibo.it/openphysicshub/en). The model code is available upon request to F.K.

Declarations

Conflict of interest The authors have no relevant financial or non-financial interests to disclose.

References

Adler RF, Sapiano MR, Huffman GJ (2018) The global precipitation climatology project (gpcp) monthly analysis (new version 23) and a review of et al (2017) (2017) global precipitation. Atmosphere 9(4):138

Amezcua J, Kalnay E, Williams PD (2011) The effects of the raw filter on the climatology and forecast skill of the speedy model. Mon Weather Rev 139(2):608–619

Armstrong McKay DI, Staal A, Abrams JF et al (2022) Exceeding 1.5 c global warming could trigger multiple climate tipping points. Science 377(6611):eabn7950

Asselin R (1972) Frequency filter for time integrations. Mon Weather Rev 100(6):487–490

Ba J, Keenlyside NS, Latif M et al (2014) A multi-model comparison of atlantic multidecadal variability. Clim Dyn 43(9):2333–2348

Balaji V (2021) Climbing down charney's ladder: machine learning and the post-dennard era of computational climate science. Phil Trans R Soc A 379(2194):20200085

Balmaseda MA, Mogensen K, Weaver AT (2013) Evaluation of the ecmwf ocean reanalysis system oras4. Q J R Meteorol Soc 139(674):1132–1161

Barnston AG, Tippett MK (2013) Predictions of nino3. 4 sst in cfsv1 and cfsv2: a diagnostic comparison. Clim Dyn 41:1615–1633

Bellucci A, Haarsma R, Bellouin N et al (2015) Advancements in decadal climate predictability: the role of nonoceanic drivers. Rev Geophys 53(2):165–202

Bellucci A, Mattei D, Ruggieri P et al (2022) Intermittent behavior in the amoc-amv relationship. Geophys Res Lett 49(17):e2022GL098771

Benassi M, Conti G, Gualdi S et al (2022) El niño teleconnection to the euro-mediterranean late-winter: the role of extratropical pacific modulation. Clim Dyn 58(7):2009–2029

Blaker AT, Joshi M, Sinha B et al (2021) Forte 2.0: a fast, parallel and flexible coupled climate model. Geosci Model Dev 14(1):275–293

Bracco A, Kucharski F, Molteni F, Hazeleger W, Severijns C (2005) Internal and forced modes of variability in the Indian Ocean. Geophys Res Lett. https://doi.org/10.1029/2005GL023154

Bracco A, Kucharski F, Molteni F et al (2007) A recipe for simulating the interannual variability of the Asian summer monsoon and its relation with enso. Clim Dyn 28:441–460

Castruccio FS, Ruprich-Robert Y, Yeager SG et al (2019) Modulation of arctic sea ice loss by atmospheric teleconnections from atlantic multidecadal variability. J Clim 32(5):1419–1441

Chen HC, Jin FF (2021) Simulations of enso phase-locking in cmip5 and cmip6. J Clim 34(12):5135–5149

Buontempo C, Burgess SN, Dee D, Pinty B, Thépaut JN, Rixen M, Almond S, Armstrong D, Brookshaw A, Alos AL, Bell B (2022) The copernicus climate change service: climate science in action. Bull Am Meteorol Soc 103(12):E2669–E2687

Di Carlo E, Ruggieri P, Davini P, Tibaldi S, Corti S (2022) ENSO teleconnections and atmospheric mean state in idealised simulations. Clim Dyn 59(11–12):3287–3304

Dobrynin M, Düsterhus A, Fröhlich K et al (2022) Hidden potential in predicting wintertime temperature anomalies in the northern hemisphere. Geophys Res Lett 49(20):e2021GL095063

Domeisen DI, Butler AH, Fröhlich K et al (2015) Seasonal predictability over europe arising from el niño and stratospheric variability in the mpi-esm seasonal prediction system. J Clim 28(1):256–271

Drijfhout S, Gleeson E, Dijkstra HA et al (2013) Spontaneous abrupt climate change due to an atmospheric blocking-sea-ice-ocean feedback in an unforced climate model simulation. Proc Natl Acad Sci 110(49):19713–19718

Drijfhout S, Bathiany S, Beaulieu C et al (2015) Catalogue of abrupt shifts in intergovernmental panel on climate change climate models. Proc Natl Acad Sci 112(43):E5777–E5786

Dunstone N, Lockwood J, Solaraju-Murali B et al (2022) Towards useful decadal climate services. Bull Am Meteorol Soc 103(7):E1705–E1719

Fasullo JT, Phillips A, Deser C (2020) Evaluation of leading modes of climate variability in the cmip archives. J Clim 33(13):5527–5545

Forest CE, Stone PH, Sokolov AP et al (2002) Quantifying uncertainties in climate system properties with the use of recent climate observations. science 295(5552):113–117

Fraedrich K, Jansen H, Kirk E et al (2005) The planet simulator: towards a user friendly model. Meteorol Z 14(3):299–304. https://doi.org/10.1127/0941-2948/2005/0043

García-Serrano J, Haarsma RJ (2017) Non-annular, hemispheric signature of the winter north Atlantic oscillation. Clim Dyn 48:3659–3670

Gong H, Wang L, Chen W et al (2016) Biases of the wintertime arctic oscillation in cmip5 models. Environ Res Lett 12(1):014001

Haarsma RJ, Campos EJ, Hazeleger W et al (2005) Dominant modes of variability in the south atlantic: a study with a hierarchy of ocean-atmosphere models. J Clim 18(11):1719–1735

Haarsma R, Acosta M, Bakhshi R et al (2020) Highresmip versions of ec-earth: Ec-earth3p and ec-earth3p-hr-description, model computational performance and basic validation. Geosci Model Dev 13(8):3507–3527

Held IM (2005) The gap between simulation and understanding in climate modeling. Bull Am Meteor Soc 86(11):1609–1614. https://doi.org/10.1175/BAMS-86-11-1609

Held IM, Suarez MJ (1994) A proposal for the intercomparison of the dynamical cores of atmospheric general circulation models. Bull Am Meteor Soc 75(10):1825–1830

Henley BJ, Gergis J, Karoly DJ et al (2015) A tripole index for the interdecadal pacific oscillation. Clim Dyn 45(11):3077–3090

Hersbach H, Bell B, Berrisford P et al (2020) The era5 global reanalysis. Q J R Meteorol Soc 146(730):1999–2049. https://doi.org/10.1002/qj.3803

Ho M, Kiem AS, Kidd DC (2012) The southern annular mode: a comparison of indices. Hydrol Earth Syst Sci 16:967–982

Holden PB, Edwards NR, Fraedrich K et al (2016) Plasim-genie v1. 0: a new intermediate complexity aogcm. Geosci Model Dev 9(9):3347–3361
Horak J, Hofer M, Gutmann E et al (2021) A process-based evaluation of the intermediate complexity atmospheric research model (icar) 1.0. 1. Geosci Model Dev 14(3):1657–1680
Hoskins BJ (1983) Dynamical processes in the atmosphere and the use of models. Q J R Meteorol Soc 109(459):1–21. https://doi.org/10.1002/qj.49710945902
Huang B, Thorne PW, Banzon VF et al (2017) Noaa extended reconstructed sea surface temperature (ersst), version 5. NOAA Natl Centers Environ Inf 30:8179–8205
Hurrel JH (1995) Decadal trends in the north atlantic oscillation: regional temperatures and precipitation. Science 269:676–679
Jeevanjee N, Hassanzadeh P, Hill S et al (2017) A perspective on climate model hierarchies. J Adv Model Earth Syst 9(4):1760–1771
Joshi M, Stringer M, Van Der Wiel K et al (2015) Igcm4: a fast, parallel and flexible intermediate climate model. Geosci Model Dev 8(4):1157–1167
Justino F, Kucharski F, Lindemann D et al (2019) A modified seasonal cycle during mis31 super-interglacial favors stronger interannual enso and monsoon variability. Clim Past 15(2):735–749
Kalnay E, Kanamitsu M, Kistler R et al (1996) The ncep/ncar 40-year reanalysis project. Bull Am Meteor Soc 77(3):437–472
Kalnay E, Sluka T, Yoshida T et al (2023) Towards strongly-coupled ensemble data assimilation with additional improvements from machine learning. Nonlinear Process Geophys Discuss 2023:1–31. https://doi.org/10.5194/npg-2023-1
Kröger J, Kucharski F (2011) Sensitivity of enso characteristics to a new interactive flux correction scheme in a coupled gcm. Clim Dyn 36:119–137
Kucharski F, Molteni F, Bracco A (2006) Decadal interactions between the western tropical pacific and the north Atlantic oscillation. Clim Dyn 26(1):79–91. https://doi.org/10.1007/s00382-005-0085-5
Kucharski F, Molteni F, King MP et al (2013) On the need of intermediate complexity general circulation models: a speedy example. Bull Am Meteor Soc 94(1):25–30
Kucharski F, Ikram F, Molteni F et al (2016) Atlantic forcing of pacific decadal variability. Clim Dyn 46(7–8):2337–2351
Lang ST, Dawson A, Diamantakis M et al (2021) More accuracy with less precision. Q J R Meteorol Soc 147(741):4358–4370
Madec G (2008) Nemo ocean engine: Note du pole de modélisation, institut pierre-simon laplace (ipsl), france, no 27 issn no 1288-1619. Technical ReportTech Rep
Maher P, Gerber EP, Medeiros B et al (2019) Model hierarchies for understanding atmospheric circulation. Rev Geophys 57(2):250–280
Marques GM, Loose N, Yankovsky E et al (2022) Neverworld2: an idealized model hierarchy to investigate ocean mesoscale eddies across resolutions. Geosci Model Dev 15(17):6567–6579
Mavilia I, Bellucci A, Athanasiadis JP (2018) On the spectral characteristics of the atlantic multidecadal variability in an ensemble of multi-century simulations. Clim Dyn 51(9):3507–3520
Mayer B, Düsterhus A, Baehr J (2021) When does the lorenz 1963 model exhibit the signal-to-noise paradox? Geophys Res Lett 48(4):e2020GL089283
McKenna S, Santoso A, Gupta AS et al (2020) Indian ocean dipole in cmip5 and cmip6: characteristics, biases, and links to enso. Sci Rep 10(1):1–13
Merryfield WJ, Baehr J, Batté L et al (2020) Current and emerging developments in subseasonal to decadal prediction. Bull Am Meteor Soc 101(6):E869–E896
Mezzina B, García-Serrano J, Bladé I et al (2020) Dynamics of the enso teleconnection and nao variability in the north atlantic-european late winter. J Clim 33(3):907–923
Mezzina B, García-Serrano J, Ambrizzi T et al (2023) Tropospheric pathways of the late-winter ENSO teleconnection to Europe. Clim Dyn 60(11–12):3307–3317
Molteni F (2003) Atmospheric simulations using a gcm with simplified physical parametrizations. i: model climatology and variability in multi-decadal experiments. Climate Dynamics 20(2):175–191. https://doi.org/10.1007/s00382-002-0268-2
Molteni F, Kucharski F, Farneti R (2023) Multi-decadal pacemaker simulations with an intermediate-complexity climate model. EGUsphere 2023:1–42
Moreno-Chamarro E, Caron LP, Loosveldt Tomas S et al (2022) Impact of increased resolution on long-standing biases in highresmip-primavera climate models. Geosci Model Dev 15(1):269–289
Nguyen H, Evans A, Lucas C et al (2013) The hadley circulation in reanalyses: climatology, variability, and change. J Clim 26(10):3357–3376
Nie Y, Scaife AA, Ren HL et al (2019) Stratospheric initial conditions provide seasonal predictability of the north Atlantic and arctic oscillations. Environ Res Lett 14(3):034006
Nof D (2008) Simple versus complex climate modeling. EOS Trans Am Geophys Union 89(52):544–545
Osborn TJ, Briffa KR, Tett SF et al (1999) Evaluation of the north Atlantic oscillation as simulated by a coupled climate model. Clim Dyn 15(9):685–702
Platov G, Krupchatnikov V, Martynova Y, et al (2017) A new earth's climate system model of intermediate complexity, plasim-icmmg-1.0: description and performance. In: IOP Conference Series: Earth and Environmental Science, IOP Publishing, p 012005
Rayner NA, Parker DE, Horton EB, Folland CK, Alexander LV, Rowell DP, Kent EC, Kaplan A (2003) Global analyses of sea surface temperature, sea ice, and night marine air temperature since the late nineteenth century. J Geophys Res Atmos 108:D14. https://doi.org/10.1029/2002JD002670
Robert AJ (1966) The integration of a low order spectral form of the primitive meteorological equations. J Meteorol Soc Japan Ser II 44(5):237–245
Ross A, Li Z, Perezhogin P, Fernandez-Granda C, Zanna L (2023) Benchmarking of machine learning ocean subgrid parameterizations in an idealized model. J Adv Model Earth Syst 15(1):e2022MS003258
Ruggieri P, Bellucci A, Nicolí D et al (2021) Atlantic multidecadal variability and north atlantic jet: a multimodel view from the decadal climate prediction project. J Clim 34(1):347–360
Ruggieri P, Benassi M, Materia S et al (2022) On the role of eurasian autumn snow cover in dynamical seasonal predictions. Clim Dyn 58(7):2031–2045
Scaife AA, Smith D (2018) A signal-to-noise paradox in climate science. npj Clim Atmos Sci 1(1):1–8
Scaife AA, Camp J, Comer R et al (2019) Does increased atmospheric resolution improve seasonal climate predictions? Atmos Sci Lett 20(8):e922
Schmittner A, Silva TA, Fraedrich K et al (2011) Effects of mountains and ice sheets on global ocean circulation. J Clim 24(11):2814–2829
Schulzweida U (2019). Cdo user guide. https://code.mpimet.mpg.de/projects/cdo/embedded/index.html
Seidenglanz A, Athanasiadis P, Ruggieri P et al (2021) Pacific circulation response to eastern arctic sea ice reduction in seasonal forecast simulations. Clim Dyn 57(9):2687–2700
Semmler T, Danilov S, Gierz P et al (2020) Simulations for cmip6 with the awi climate model awi-cm-1-1. J Adv Model Earth Syst 12(9):e2019MS002009
Sluka TC, Penny SG, Kalnay E et al (2016) Assimilating atmospheric observations into the ocean using strongly coupled ensemble data assimilation. Geophys Res Lett 43(2):752–759

Smith RS, Gregory JM, Osprey A (2008) A description of the famous (version xdbua) climate model and control run. Geosci Model Dev 1(1):53–68. https://doi.org/10.5194/gmd-1-53-2008

Smith D, Eade R, Scaife AA et al (2019) Robust skill of decadal climate predictions. Npj Clim Atmos Sci 2(1):1–10

Smith DM, Scaife AA, Eade R et al (2020) North Atlantic climate far more predictable than models imply. Nature 583(7818):796–800

Tondeur M, Carrassi A, Vannitsem S et al (2020) On temporal scale separation in coupled data assimilation with the ensemble kalman filter. J Stat Phys 179(5–6):1161–1185

Trenberth KE, Shea DJ (2006) Atlantic hurricanes and natural variability in 2005. Geophys Res Lett. https://doi.org/10.1029/2006GL026894

Tyrrell NL, Karpechko AY (2021) Minimal impact of model biases on northern hemisphere el niño-southern oscillation teleconnections. Weather Clim Dyn 2(3):913–925

Valcke S (2013) The oasis3 coupler: a European climate modelling community software. Geosci Model Dev 6(2):373–388

Walsh J, Chapman W, Fetterer F, et al (2019) Gridded monthly sea ice extent and concentration, 1850 onward, version 2.[sea ice concentration]. Boulder, Colorado USA NSIDC: National Snow and Ice Data Center Accessed 9 July2022

Wang B, Ding Q (2008) Global monsoon: dominant mode of annual variation in the tropics. Dyn Atmos Oceans 44(3–4):165–183

Wang B, Kim HJ, Kikuchi K et al (2011) Diagnostic metrics for evaluation of annual and diurnal cycles. Clim Dyn 37(5):941–955

Weber SL (2010) The utility of earth system models of intermediate complexity (emics). Wiley Interdiscip Rev: Clim Change 1(2):243–252

Wild M (2020) The global energy balance as represented in cmip6 climate models. Clim Dyn 55(3–4):553–577

Williams J, Totterdell I, Halloran P et al (2014) Numerical simulations of oceanic oxygen cycling in the famous earth-system model: Famous-es, version 1.0. Geosci Model Dev 7(4):1419–1431

Xie P, Arkin PA (1997) Global precipitation: a 17-year monthly analysis based on gauge observations, satellite estimates, and numerical model outputs. Bull Am Meteor Soc 78(11):2539–2558

Yang C, Christensen HM, Corti S et al (2019) The impact of stochastic physics on the el niño southern oscillation in the ec-earth coupled model. Clim Dyn 53:2843–2859

Zebiak SE (1993) Air-sea interaction in the equatorial Atlantic region. J Clim 6(8):1567–1586

Zhang W, Kirtman B, Siqueira L et al (2021) Understanding the signal-to-noise paradox in decadal climate predictability from cmip5 and an eddying global coupled model. Clim Dyn 56:2895–2913